 CMES, vol.3, no.5, pp.675-685, 2002

Bonding Geometry and Bandgap Changes of Carbon Nanotubes Under Uniaxial and Torsional Strain

Liu Yang[1], Jie Han, M. P. Anantram, and Richard L. Jaffe

Abstract: Bonding geometry and bandgap of carbon nantotubes under uniaxial and torsional deformation are studied computationally for nanotubes of various chiralities and diameters. Bonding geometries are obtained with Tersoff-Brenner potential from molecular mechanics simulations. Bandgaps as function of strain are calculated from the molecular mechanics structures using one (p) and four (2s and $2p_x$, $2p_y$, $2p_z$) orbital tight-binding models. For small strains, the bandgap results are qualitatively consistent with those predicted by the one orbital analytical model. Response of the electronic properties of nanotubes to large strains is characterized by a change in sign of *d(bandgap)/d(strain)*. These originate from either quantum number or bonding geometry effects, and are strain-induced semiconductor-metal transitions. The effect of variations in bonding geometries between continuum mechanics and molecular mechanics structures on the electronic properties and differences between the one and four orbital models are also presented.

1 Introduction

The interesting electronic and mechanical properties of carbon nanotubes are due to their simple and elegant relationships with their well-defined tube geometry. A single-walled nanotube can be considered as a seamless rolled graphene sheet. Its geometry is well defined by a chiral vector (n_1, n_2) on the sheet ($\Delta n = n_1 - n_2 > 0$), or equivalently the tube diameter and chiral angle (d, ϕ). A tube is metallic if mod(Δn, 3) = 0 and semiconducting otherwise. The bandgap of a semiconducting tube is 1/d dependent, and typically around 1 eV for a tube with a diameter of 1 nm. These properties were predicted by applying the one p-orbital tight-binding model of the graphene sheet to nanotubes[Mintmire, Dunlap, White (1992); Hamada, Sawada, Oshiyama (1992); Saito, Fujita, Dresselhaus, Dresselhaus (1992)], and confirmed by first-principles, local density approximation (LDA) calculations [Mintmire, White (1995); Louie (1996)] and also experiments [Wildoer, Venema, Rinzler, Smalley, Dekker (1998); Odom, Huang Kim, Lieber (1998)].

The mechanical properties of carbon nanotubes are characterized by an extremely high Young's modulus of $\sim$1 TPa [Robertson, Brenner, Mintmire (1992); Dai, Hafner, Rinzler, Colbert, Smalley (1996); Lu (1997)]. A variety of mechanical deformations, including stretching, compressing, twisting, bending, and buckling, have been observed and studied [Yakobsen, Brabec, Bernhoc (1996); Falvo, et al. (1997)]. The nanotube stress-strain relations were found to follow the continuum mechanics of column beams. The mechanical deformations were correlated to Young's modulus and tube geometry (diameter and length). Beyond the linear range, nanotubes exhibit an extraordinary elastic response. For example, nanotubes were found to respond elastically to strains as high as 20 - 30% by undergoing buckling[Falvo, et al. (1997)]. The elastic recovery from buckling during nanotube tip based nanolithography was observed experimentally [Dai, Franklin, Han (1998)] and studied by molecular dynamics simulations [Garg, Harg, Sinnot (1998)].

Theoretical efforts have been made to correlate electronic and mechanical properties of nanotubes under uniaxial and torsional deformations. These two deformation modes correspond to the in-plane tension and shear of graphene sheets. Their electronic responses can be predicted analytically as was done for the perfect tubes. Heyd et al. (1997) studied the effects of uniaxial stress on bandgap of zig-zag tubes by applying hopping parameters scaled by bond lengths with one orbital tight-binding model, and by assuming continuum mechanics linear scaling to the bond lengths. Kane and Mele (1997) predicted the effects of torsion on bandgaps of armchair

[1] liuyang@pegasus.arc.nasa.gov
NASA Ames Research Center
Mail Stop 230
Moffett Field, CA 94035

tubes by an alternative approach which wraps a massless two dimensional Dirac Hamitonian on a curved surface.

Recently, we developed a theoretical framework based on a Huckel tight-binding model to explain the electronic structure change of carbon nanotubes with arbitrary chirality [Yang, Han (2000)]. A graphene sheet possesses a hexagonal Brilloin zone in the reciprocal space (Fig. 1) because of its hexagonal lattice structure. Due to the quasi-one dimensional nature of nanotubes, the allowed electronic states for carbon nanotubes formed parallel k lines in the reciprocal space. For an undeformed carbon nanotube, the Fermi point k_F is coincident with the vertex of the hexagonal Brilloin zone. The chiral vector, more specifically mod(Δn,3), determines if the Fermi point k_F sits on one of the k lines. The distance between parallel k lines is proportional to 1/d. And the relative position between k_F and the k lines is critical to the electronic structure of the tube. When mod(Δn,3)=0, k_F sits on one of the k lines, and the tube is conducting. Otherwise it is semiconducting and k_F sits in between two k lines. The bandgap is proportional to the distance from the Fermi point k_F to the closest k line.

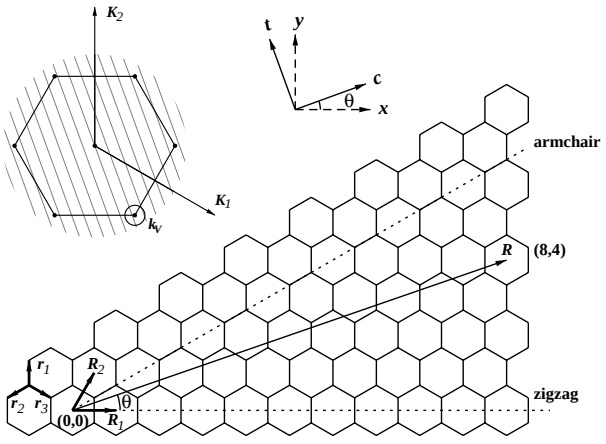

Figure 1 : Graphite lattice and hexagonal central Brillouin zone with reciprocal vectors k_1 and k_2, and k parallel lines for allowed electronic states.

A uniform uniaxial or torsional deformation applied to a nanotube causes the Fermi point k_F to shift away from the Brillion zone vertex. The amplitude of this shift is proportional to the strain and the direction of this shift, relative to the k lines, is determined by the deformation mode and tube chirality. When k_F shifts parallel to the k lines, as in the case of an armchair tube under tension/compression, or a zigzag tube under torsion, the deformation does little to the band gap. On the other hand, when the k_F shift is not parallel to the k lines, it results in substantial changes in the tube electronic properties, including shifting, merging, and splitting of the Van Hove singularities of the density of states, and a change in the bandgap. When k_F shifts towards the closest k line, for instance, for a mod(Δn,3)=1 tube under compression, or a mod(Δn,3)=-1 tube under tension, the bandgap increases initially. For these tubes, the first pair of density of states peaks moves towards each other. The other pairs of peaks moves in alternate directions. When k_F hits the closest k line, the DOS peaks merge and the band gap disappears. When k_F moves further under an increased strain. The bandgap appears again, as well as a pair of new DOS Van Hove singularities peaks. For other combinations of tube chirality and deformation mode, similar changes in electronic properties occur. How much the electronic properties change with deformation is determined by the angle of the k_F shift direction and the k lines.

This analysis was based on the assumption that the tube geometry scales linearly with the strain, and that only the first order effects are important. Thus, the results are only expected to be valid for small strains. However, one of the important properties of nanotubes is their elastic response to large mechanical deformations. It is of interest to extend the previous work to large deformations. The electronic response to large strains can be as extraordinary as the mechanical response. For example, it was predicted that a semiconductor-to-metal transition [Hyed, Charlier, McRae (1997)] and a sudden change in bandgap [Yang, Han (2000)] could be induced by large strains. The one p-orbital tight-binding approach and continuum mechanics are good methods to predict the electronic and mechanical properties of nanotubes, respectively. However, they need to be verified when applied to highly deformed nanotubes. Continuum mechanics enables linear scaling of the bonding geometries of slightly strained nanotubes. But its linear scalability is questionable for largely deformed nanotubes. In addition, the effect of curvature induced $s-p$ hybridization in largely deformed tubes may need to be considered.

Solution to these problems is to obtain the relaxed atomic structures and testing their effects on the electronic properties. We employ molecular mechanics simulations and one and four orbital tight-binding calculations here. De-

tails of our approach are in described in Section 2 Sec. 3 contains molecular mechanics results for bonding geometries changes of nanotubes under large uniaxial and torsional deformations. These results are used to bridge mechanical and electronic properties of deformed tubes. In Sec. 4, the tight-binding methods are applied to modeling the electronic properties of the deformed carbon nanotubes based on the molecular mechanics relaxed structures. Extraordinary electronic responses, including metal - semiconductor transitions, are revealed and related to changes in quantum numbers and bonding geometries. Conclusions are presented in Sec. 5.

2 Methods

The simulation of nanotube deformation is a two step process. First, the perfect nanotube is deformed to the desired strain by scaling as described below, and then molecular mechanics simulation is used to allow the nanotube to relax under the strain. The Tersoff-Brenner many body potential is used for the molacular mechanics simulation. This potential describes the atomic interactions through the stretch, bend and torsion of chemical bonds in carbon systems, including C-C bond breaking and fraction. It has been widely employed in studying atomic structures and mechanical properties of nanotubes due to its success in reliable and efficient computation of large carbon systems [Robertson, Brenner, Mintmire (1992); Yakobsen, Brabec, Bernhoc (1996); Garg, Han, Sinnot (1998)].

The simulations start with a rolled graphene sheet. For uniaxial deformation, all the atom positions and tube length are linearly scaled by the given amount of strain along the tube axis. For torsional deformation, all the atom positions rotate around the tube axis by an angle determined by the given strain along the circumference. To eliminate the end effects, periodic boundary conditions are applied in the axial direction. This is straightforward for uniaxial deformation, but involves a two step operation for torsional deformation: a translation by the tube length followed by a rotation by the torsional angle. For the torsional case, the length is properly chosen so that when the periodic boundary condition is applied to the system, the atoms can stack smoothly across the boundary.

To characterize the bonding geometries, we denote three bonds associated with an atom as a, b, and c in the order from the closest to the tube axis to the closest to the tube circumference (see Fig. 2). The average of the distance from all the atoms to the tube center is taken as the tube diameter. The uniaxial strain is defined as the tube length change divided by the tube length. The positive and negative values are chosen to represent the tensile and compressive strains, respectively. The torsional strain is expressed as the conventional shear strain, a ratio of the rotating distance along the circumference to the tube length. The positive and negative values are arbitrarily chosen to represent the clockwise and counter-clockwise torsional deformations.

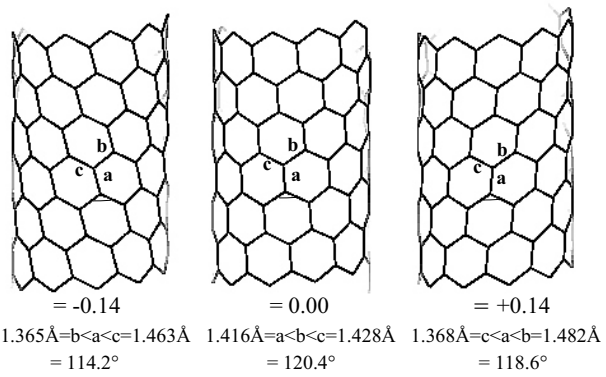

Figure 2 : Molecular models of a (10, 1) nanotube unit under clockwise (.14 strain), zero, and counter-clockwise strains (-.14 strain), obtained from molecular mechanics simulations.

We employ one and four orbital tight-binding approaches to examine the electronic responses to the mechanical deformation of nanotubes. The four orbital model includes the effects of tube curvature and distortions to the *s*and*p* states that are ignored in the one orbital model. A minimum basis of atomic *s* and *p* valence orbitals $(2s, 2p_x, 2p_y, 2p_z)$ is utilized in the one and four orbital model. Values for the on-site and hopping matrix elements are taken from Mintmire and White (1995). They were calibrated by fitting to first-principles electronic structures of fullerenes, nanotubes and other hydrocarbon-based materials. The effects of variation in bonding geometries on electronic properties of deformed tubes are included in the one and four orbital calculations. This is done by using Harrison's approach [Harrison (1980)] to scale hopping parameters by $(r_0/r)^2$ where*r*is the bond length with r_0 = *1.42 Å*. This scal-

ing method was also employed in studying electronic response to mechanical deformations by other researchers [Hyed, Charlier, McRae (1997)] and us [Yang, Han (2000)].

Model nanotubes used in this work are listed in Table 1. Tube diameter varies from 0.7 to 1.1 nm. Repeat units determined by tube chiral and translation vectors are used for tight-binding calculations. Several repeat units are employed in molecular mechanics simulations to ensure that the tube length is larger than the potential cutoff ($\sim$0.2 nm).

3 Bonding Geometries of Deformed Carbon Nanotubes

Under compression and torsion, the stress - strain ($\sigma-\varepsilon$) curves of nanotubes exhibit a linear behavior followed by a series of nonlinear responses with varied buckles [Yakobsen, Brabec, Bernhoc (1996)]. In contrast, nanotubes under tension do not buckle, and continue the elastic deformation until bonds break. In this work, deformations are limited to a strain range with no buckle or singularity in the stress - strain curves. In this strain range, nanotubes have a stable atomic structure and a smooth cylindrical shapes. The bonding geometries and tube diameter are uniform.

The strain at which compression buckling starts depends on the tube diameter and chirality. It also depends on the time allowed for the tube to relax and the length of the tube repeat unit. We also systematically examined the buckling strain of single-walled carbon nanotubes in other publications. Since it is not the focus of this publication, we discuss in general what the bonding geometry would be for the tube to keep a uniform configuration up to 12-14% of compressive strain. The maximum strain during elongation is taken as 25%, smaller than the 40% beyond which the tight-binding model no longer describes atomic interactions. Similar situations exist for the buckling strain under torsion. The two buckling strains in clockwise and counter-clockwise rotational deformations are equivalent for symmetric (zigzag and armchair) tubes, but different for unsymmetrical (chiral) tubes. We examine the uniform torsional strain up to 14 $\sim$ 18% for nanotubes listed in Table 1. Shown in Fig. 2 are molecular mechanics structures of a (10, 1) nanotube at clockwise torsion (- 0.14), zero, and counter-clockwise torsion (+0.14) strains. In this range, the stable structures exhibit well defined tube and bonding geometries. That is, bond lengths (a, b, c) and angle and tube radius keep the same value for each atom.

As an example, the variation in bonding geometry of (10,1) nanotube under uniaxial and torsional deformations are shown in Fig. 3 and Fig. 4. It is easy to see that $a = b = c$ *(1.42 Å)* for a graphene sheet, but the a, b and c bonds are not equivalent for a rolled-up sheet, i.e. a nanotube. All the bonds could keep the same length if one argues, for example, the rolled-up sheet is a polygonal geometry with bonds laying on the surface. However, we find after relaxation $a < b < c$ (ε = 0), with $a = b < c$ for armchair tubes, $a < b = c$ for zigzag tubes, and $a < b < c$ for chiral tubes including the (10, 1) tube in Fig. 2. This can be explained as follows: the strain in the rolled-up sheet is concentrated on the tube circumference, and originates from the crowded atomic packing in this direction. Energy minimization with the tube length constraint will maximally increase bond c to compensate both the bond shortening and curvature effect. This leads to $a < b < c$. It must be noted however, that this relationship may vary among different energy minimization and constraint approaches. For example, a short tube without tube length constraint could exhibit the largest bond length along the tube axis, leading to $a > c$.

When subjected to uniaxial deformations, it can be expected that $da/d\varepsilon > db/d\varepsilon > dc/d\varepsilon$ as bonds $a, b,$ and c are defined in the order from the closest to the tube axis (uniaxial stress direction) to the closest to the tube circumference. This leads to a change from $a < b < c$ (ε = 0) to $a = b = c$ $\varepsilon \sim$ 1% in Fig. 3), and to $a > b > c$, and is driven by tension. In contrast, compression can cause a change from $a > c$ to $a = c$, and to $a < c$. Fig. 3 also shows that $d(a-c)/d\varepsilon$ changes from positive to negative at a large tensile strain (18%). This is due to an increase in energy from the minumum at the equilibrium bond length to the position of the barrier for bond breaking during bond stretching in tension. When the strain approaches the barrier for bond breaking, the $a/d\varepsilon$ will decrease to zero unless a much higher energy is provided to break the bond. In contrast, the $dc/d\varepsilon$ will increase because bond c is still far away from the barrier. In the compression side, we could not observe this due to the limited strain. For all the model nanotubes in Table 1, we find that $a = b = c$ at 1 - 2% tensile strains and $d(a-c)/d\varepsilon$ changes sign at 17 - 18% tensile strains. We will see that these variations in bonding geometries are strongly related to electronic response to strains.

Table 1 : Model Nanotubes

chirality (n_1, n_2)	mod(Δn, 3)	m (= Δn - 3q)	type
(5, 5), (7, 7) (9, 0), (10, 1)	0	0	metal I (MI) ($n_1 = n_2$) metal II (MII) ($n_1 \neq n_2$)
(6, 5), (10, 0), (8, 1)	1	1	semiconductor I (SI)
(7, 5), (8, 0), (9, 1)	2	-1	semiconductor II (SII)

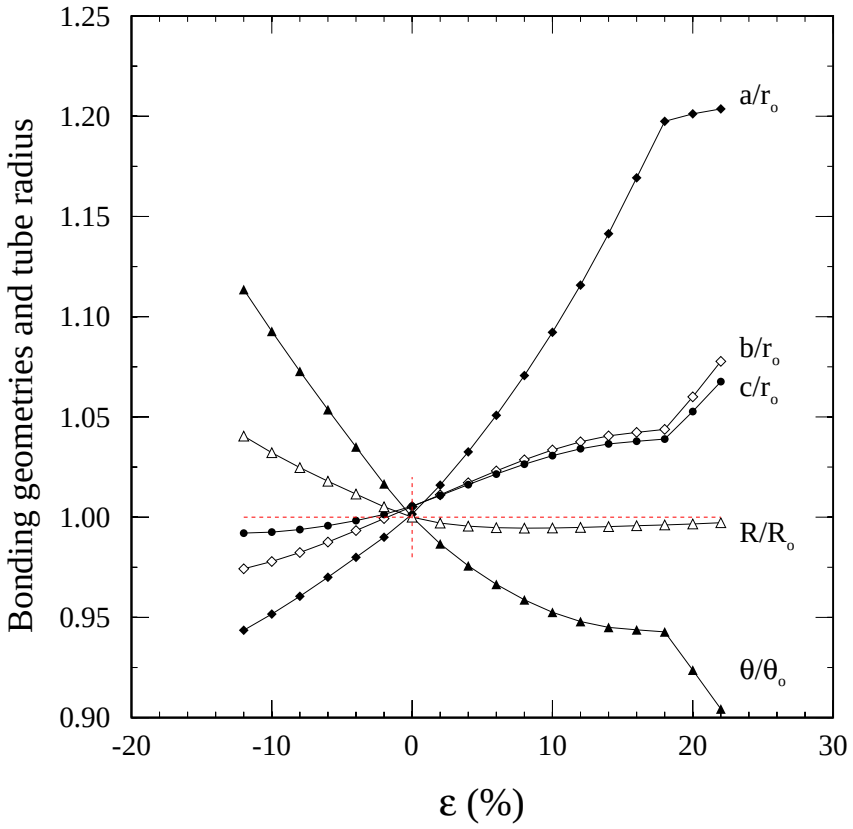

Figure 3 : Bond lengths, angle and tube radius as functions of tension (> 0) and compression (< 0) strain for (10, 1) nanotube shown in Fig. 2. They are scaled, respectively, by 1.42 Å, 120°, and the tube radius at zero strain.

In contrast to the uniaxial deformation, torsional deformation presents complicated variations in bonding geometries as this deformation breaks both tube and bonding symmetry. In uniaxial deformation, $da/d\varepsilon > db/d\varepsilon > dc/d\varepsilon > 0$, leading to a change from $a < b < c(\varepsilon = 0)$ to $a = b = c(\varepsilon = 1\%)$, and to $a > b > c$. In torsional deformation, as shown in Fig. 4, $db/d\varepsilon > 0$ but $da/d\varepsilon < dc/d\varepsilon < 0$, and consequently that $b = c$ or $a = b$ or $a = c$ at some strains, but never $a = b = c$. Owing to similar changes in bond lengths of other nanotubes, the condition $a = b = c$ is impossible under torsional deformation. It also can be seen from Fig. 4 that the tube diameter and the angle between bonds *b* and *c* decreases due to torsional strain along the tube circumference.

The simulations show that the maximum bond strain, qualitatively, is $(1 - n_2/n_1)$ and n_2/n_1 dependent, respectively, under uniaxial and torsional deformations. This is because the stress on the bond, and therefore the bond strain, is proportional to $cos\phi$ (~ 1-n_2/n_1) and $sin\phi$ ($\sim n_2/n_1$) for these two cases. These dependences can be understood from Fig. 2 with the chiral angle ϕ between the tube circumference (torsion stress direction) and the vector perpendicular to bond *a*, or equivalently between the tube axis (tensile stress direction) and bond *a*. We also can take bond *a* and *c* as representatives of bonds of zigzag and armchair tube (n_2/n_1=0 and 1, ϕ = 0 and 30°), respectively. Thus, the $da > dc$ in Fig. 3 and $|dc| > |da|$ in Fig. 4 illustrate the dependence of the bond strain

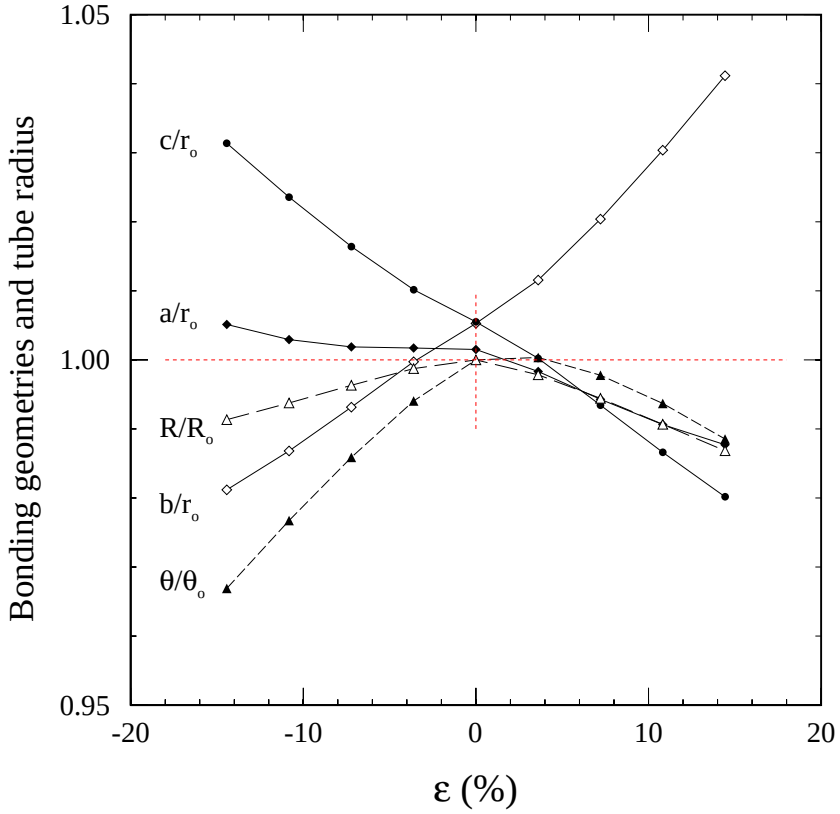

Figure 4 : Bond length, angle, and tube radius as functions of counter-clockwise (>0) and clockwise (<0) torsional strain for (10, 1) nanotube shown in Fig. 2. They are scaled, respectively, by 1.42 Å, 120°, and the tube radius at zero strain.

on tube chirality under tensile and torsion deformations. From a series of simulations for zigzag (9, 0) to armchair (5, 5) tubes, the maximum bond strain changes from 0.11 to 0.07 under tensile, but from .01 to .05 under torsion at 10% tube strains as n_2/n_1 increases from 0 to 1.

We now turn to the nonsymmetrical change during tensile and compression strain in Fig. 3. An increase in tube diameter during compression is favored by energy minimization. But a decrease in tube diameter during tension is not. This leads to the observation that tube diameter changes more in compression, and less in tension. The nonsymmetrical aspects and the scalability of continuum mechanics to bonding geometries and tube diameter are further validated in Fig. 5. The scaling relations of continuum elastic mechanics are represented by two dashed lines, respectively, for the tube axial component in bond lengths and the tube cross section area. The continuum model deviates from the results of the molecular mechanics (solid lines) especially for bonding geometries in compression ($\varepsilon < 0$) and for tube diameter in tension ($\varepsilon > 0$). It appears that conservation of volume on which the continuum elastic mechanics model is based, is not generally found for deformed nanotubes.

It can be expected that variations in bonding geometries and tube diameter under mechanical deformations will determine response behavior of electronic properties of nanotubes to the deformations. This is explored in the following section.

4 Bandgap Changes of Deformed Carbon Nanotubes

We first compare the one and four orbital tight-binding calculations for a molecular mechanics relaxed (9, 0) nanotube. The computed bandgap E_g versus uniaxial strain curves are shown in Fig. 6. The (9, 0) tube has a small bandgap at zero strain while the one orbital

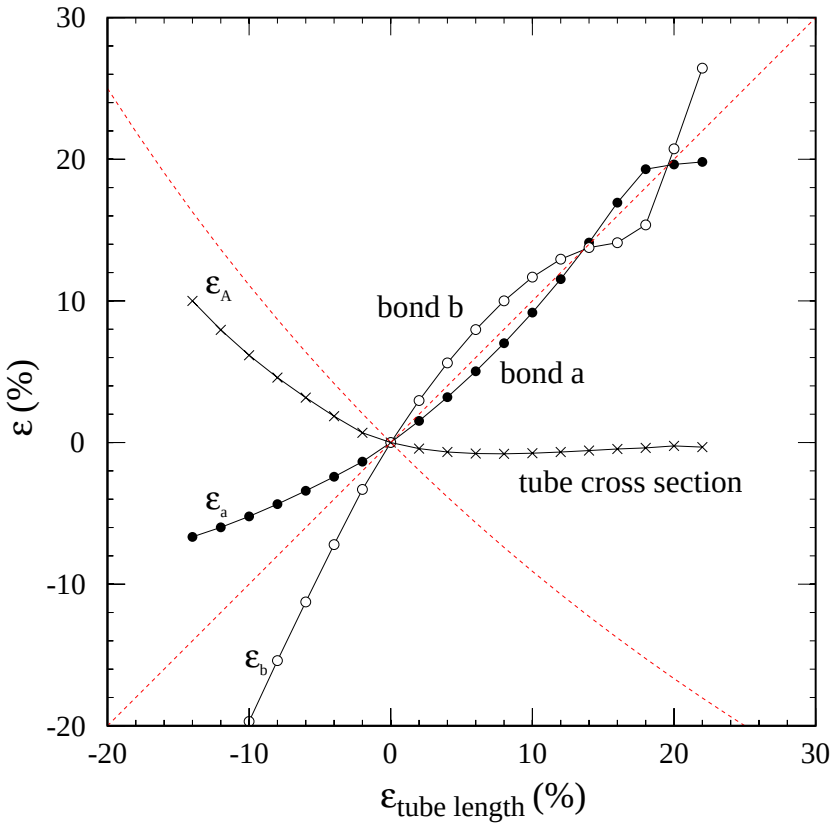

Figure 5 : Comparision in strains of bond lengths and tube cross section between continuum mechanics (dashed lines) and molecular mechanics (solid lines) structures for a (8, 0) nanotube under compression (< 0) and tensile (> 0) deformations.

model based on graphene sheet with equal bond lengths predicted a zero bandgap. Our four orbital model of the unrelaxed structure predicts a small gap of 0.1 eV for (9,0) tube, in agreement with results obtained from LDA and first-principle calculations nanotubes with unrelaxed structure [Louie (1996); Wildoer, Venema, Rinzler, Smalley, Dekker (1998)]. In those papers, the nonzero bandgap was attributed to curvature induced $s-p$ hybridization (or simply, the curvature effect). In addition, the relaxed bonding geometry (i.e. a ≠ c) causes an extra gap of 0.1 eV by the one orbital model of the relaxed structure. It seems that the bandgap (0.2 eV) obtained from the four orbital model of the relaxed structure can be estimated by a sum of that (0.1 eV) of one orbital model of the relaxed structure (the bonding geometry effect) and that (0.1 eV) of the four orbital model of the unrelaxed structure (the curvature effect).

Under tensile strain ($\varepsilon > 0$), the bonding geometries change from $a = b < c$ to $a = b = c$, and consequently the bandgap decreases to zero at ε = 1%, as shown by the one orbital model of the relaxed structure. In contrast, this also can be reached by a compression in that bonding geometries change from $a = b > c$ to $a = b = c$, as Heyd et al showed (1997). A measurement shows that $|dE_g/d\varepsilon|$ is larger in tension than in compression (about 0.07 vs. 0.04 eV) in the one orbital model calculations. This is indicative of a tube diameter effect on bandgap ($\sim d^{-1}$), because the tube diameter increases significantly in compression, and decreases slightly in tension (Fig.2). As a result, the bandgap increase is more slowly with increase in compression strain rather than tensile strain. The rate of bandgap change for compression is slightly higher in one orbital model than in four orbital model because of an extra curvature effect caused by changes in

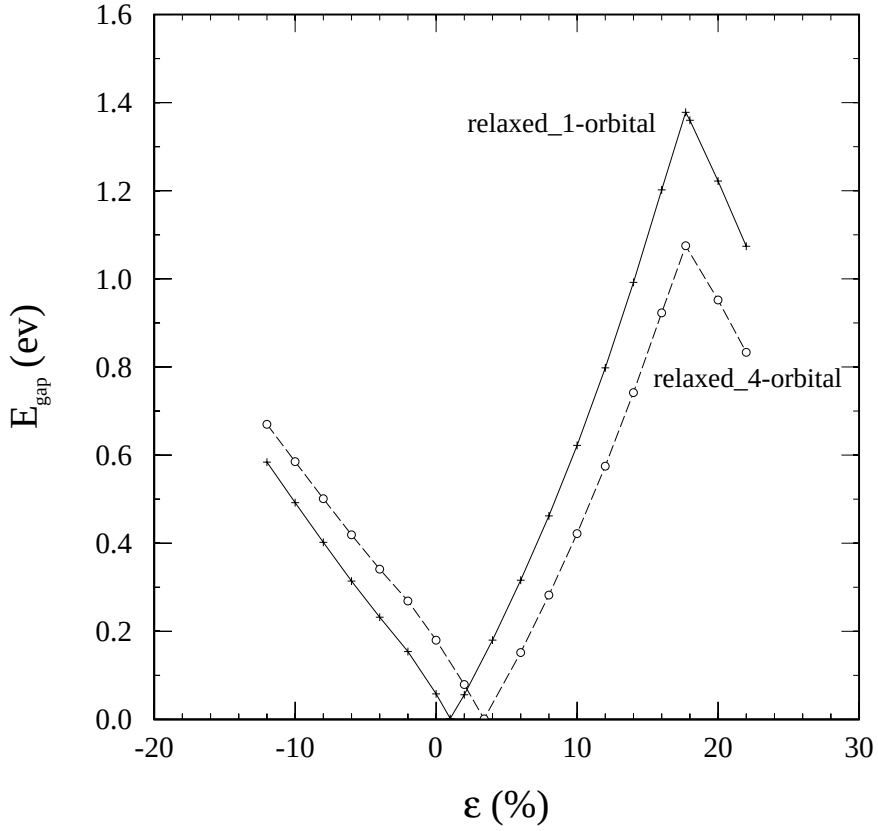

Figure 6 : Bandgaps of a (9, 0) nanotube as functions of compression (<0) and tensile (>0) strain, calculated from one and four obital models.

tube diameter. However, over a wide range of strains, the bandgap from four orbital model can be obtained approximately by shifting one orbital model with 2% higher strain. With continue increase in tensile strain, we see a decrease in the band gap, or $dE_g/d\varepsilon$ change its sign at 18% strain, for both the one and four orbital models. The observed change in sign of $d(a-c)/d\varepsilon$ at 18% strain for the molecular mechanics structure is responsible for the change in the bandgap.

By taking the (9, 0) tube under uniaxial deformation as an example, we illustrated three effects of geometry relaxation on bandgap. They include three effects. One is the curvature effect (s-p hybridization) revealed by four orbital model. It contributes a 0.1 eV gap with a slight change as a function of the tube curvature or strain. The other two are the diameter effect related to the number of atoms along the tube circumference, and geometry relaxation effect. They are included in both one and four orbital models. The bandgap results based from the four orbital model can be approximated by those of the one orbital model with a correction for the curvature effect. In the following discussion, we will focus on results obtained from the one orbital model for relaxed molecular mechanics structures keeping in mind of the effects of curvature.

The results obtained from one orbital tight-binding calculations are shown in Fig. 7 and 8, respectively, for model tubes in Table 1 under uniaxial and torsional strain. The bandgap is scaled by the product of the unrelaxed tube radius, a bond length (1.42 Å) and a hopping parameter (2.64 eV). At small strains up to $\pm 10\%$, the results based on molecular mechanics structures are qualitatively consistent with those based on continuum mechanics analysis. That is, $dE_g/d\varepsilon$ is positive and negative, respectively, for SI and SII types of semiconducting tubes (see Table 1) under uniaxial deformation, and the opposite is true under torsional deformations. For nanotubes under uniaxial deformations $|dE_g/d\varepsilon|$ is $cos3\phi$ dependent,

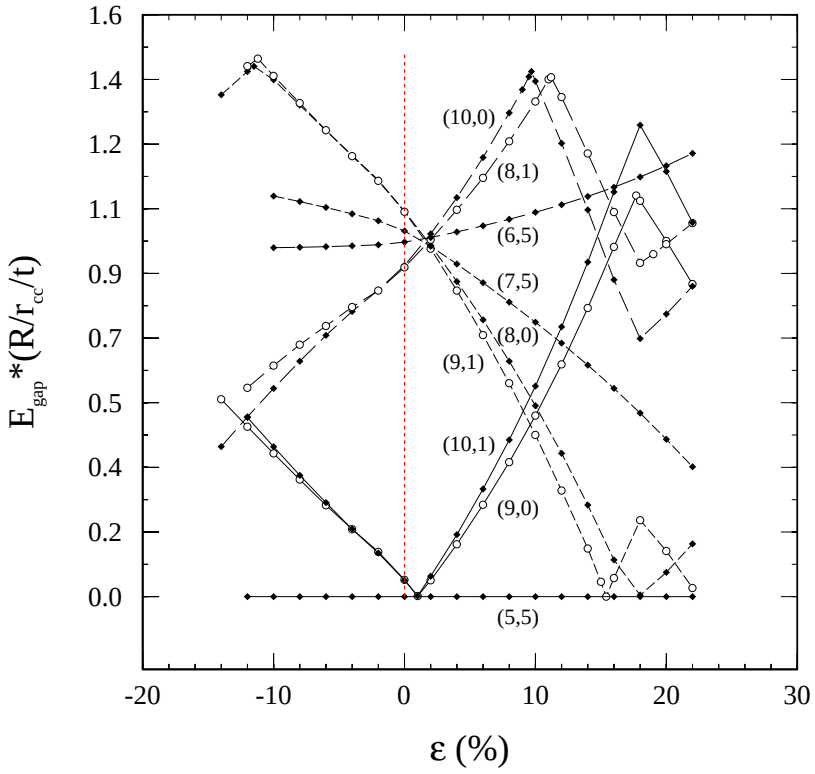

Figure 7 : Bandgaps of various nanotubes as functions of compression (< 0) and tensile (> 0) strain, obtained from one orbital tight-binding calcualtions of molecular mechancis structures. They are scaled by tube radius, bond length (1.42Å) and hopping parameter (2.64 eV).

qualitatively, increasing from zero for armchair tubes to a maximum for zigzag tubes. In contrast, $|dE_g/d\varepsilon|$ is $sin3\phi$ dependent, qualitatively, under torsional deformation, reaching a minimum (zero) for zigzag tubes, and maximum for armchair tubes. The dependence of $|dE_g/d\varepsilon|$ on tube chirality obviously follows the dependence of the maximum bond strain on tube chirality, as discussed in Sec. 3.

In addition, there are some interesting features that were not addressed in the previous work. For example, the small bandgap at zero strain for (9, 0), caused by $c > a$, is eliminated by a 1% tensile strain (Fig. 7) at which $a = b = c$, but, it cannot be eliminated by the bonding geometry effect for torsional deformation because there is no strain with $a = b = c$. However, the bandgap of (10, 1) tube reaches zero at 1% tensile strain (Fig. 7), and also at -8% torsional strain (Fig. 8). The change in the sign of $dE_g/d\varepsilon$ at a large strain highlights a feature of the electronic properties of nanotubes under large deformations.

We now take a closer look at the strain, ε_c, at which $dE_g/d\varepsilon$ changes sign. There are various such strains in Fig. 7 and 8 at large deformations. They represent an extraordinary response of electronic properties of nanotubes to large deformation. We classify them into two types. First, there exists and ε_c at which E_g is zero. This strain defines a transition between semiconductor and metal. It is zero for metallic or armchair tubes (MI type), as illustrated by a (5, 5) tube under torsional strain in Fig. 8. It is near zero (1% tensile strain) for zigzag metallic (MII type) tubes such as (9, 0) and (10, 1) tubes (Fig. 7). Semiconducting tubes also show this strain at a large value, for example, around 16% and 18%, respectively, for tubes (9, 1) and (8, 0) under tensile deformation (Fig. 7). These results confirm the our prediction for the transition of SII type of tubes from semiconductor to metal under tensile deformation [Yang, Han (2000)].

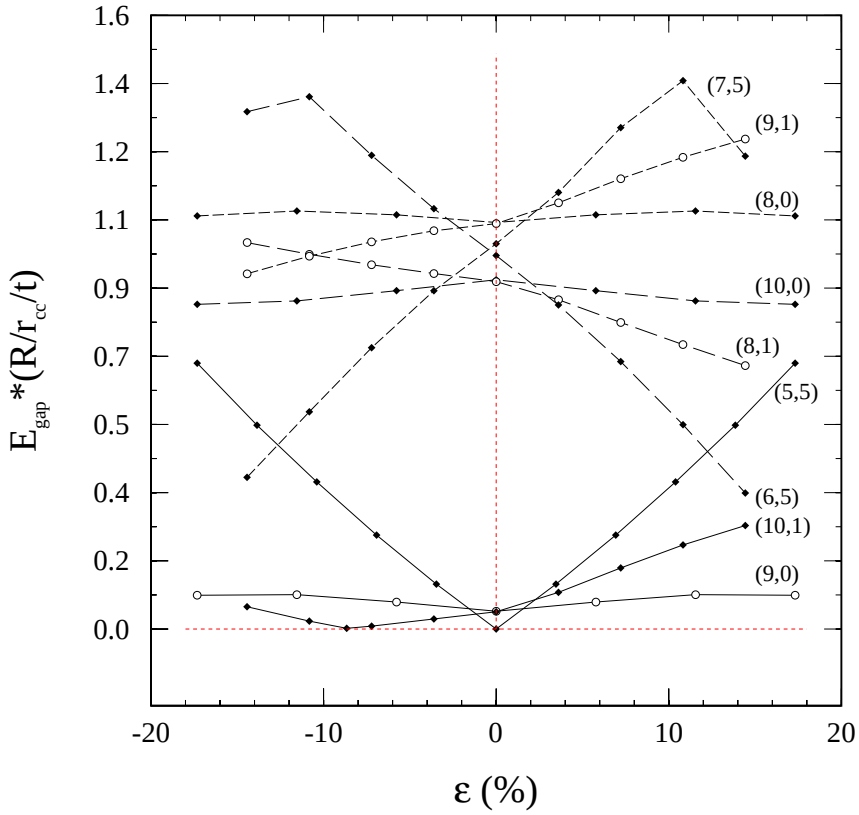

Figure 8 : Bandgaps of various nanotubes as functions of clockwise (< 0) and counter-clockwise (> 0) strain, obtained from one orbital tight-binding calcualtions of molecular mechancis structures. They are scaled by tube radius (Å), bond length (1.42Å) and hopping parameter (2.64 eV).

However, the predicted transition for SI type tubes such as (10, 0) and (8, 1) under compression cannot be observed within the studied elastic deformation range. Beyond this range, unstable buckles appear and may prevent the bandgap from reaching zero (see Fig. 7). For convenience, we call this type of strain as metal - semiconductor transition strain.

The second type of ε_c includes those at which $E_g > 0$. Semiconducting tubes (8, 0), (9, 1), (8, 1) and (10, 0) in Fig. 7, and (6, 5) and (7, 5) in Fig. 8 exhibit this strain at about $\pm$10%. In contrast, tubes (9, 1), (8, 1), (10, 0), (9, 0) and (10, 0) under tensile display this strain around 18%. As mentioned in the discussion of Fig. 6, the ε_c = 18% is attributed to the bonding geometry effects which cause $d(a-c)/d\varepsilon$, and consequently $dE_g/d\varepsilon$ to change sign. A value of ε_c = 10% was reported for tube (10, 0) under tensile deformation and attributed to the quantum number effect [Yang, Han (2000)]. This effect can be understood by a crossover of quantum number q in a strain dependent dispersion relation $E(q,k)$. Strain drives k_F shifting among the k lines in the reciprocal space. This leads to a change in quantum number and $dE_g/d\varepsilon$. We carried out a one orbital calculation for tube (10, 0) strained by continuum mechanics, and found a sign change only at 10%, confirming that these two strains, 10% and 18%, originate from quantum number and bonding geometry effects, respectively.

5 Conclusion

Molecular mechanics simulations provide insights into variations in bonding geometries and tube diameter of nanotubes under uniaxial and torsional deformations. They do not always follow the scaling relations of continuum mechanics. The one and four orbital tight-binding calculations of molecular mechanics structures confirm the prediction of response of electronic properties of nanotubes to small deformations. That is, $dE_g/d\varepsilon$ is positive

and negative, respectively, for nanotubes with $\Delta n = 3q + 1$ and $3q - 1$ under uniaxial deformation. In contrast, the opposite is true under torsional deformation. Qualitatively, The $|dE_g/d\varepsilon|$ and the maximum bond strain are $cos3\phi$ and $sin3\phi$ dependent, respectively, under uniaxial and torsional deformations. Response of electronic properties of nanotubes to large deformations are characterized by two other types of transition strains. One signifies a strain induced metal - semiconductor transition at which $E_g = 0$, and the other is originated from either quantum number effect or bonding geometry effect at which $E_g > 0$. The strain induced metal - semiconductor transitions can occur for various nanotubes under both uniaxial and torsional deformations within one orbital model. But, this occurs only for armchair tubes under torsion as other tubes will remain a finite small bandgap because of the intrinsic curvature effect.

References

Anantram, M.P.; Govindan, T.R. (1998): *Phys. Rev. B.*, **58**, 4882.

Brenner, D.W. (1990): *Phys. Rev. B*, **42**, 9458.

Dai, H.; Franklin, N.; Han, J. (1998): *Appl. Phys. Lett.*, **73**, 1508.

Dai, H.; Hafner, J.H.; Rinzler, A.G.; Colbert, D.T.; Smalley, R.E. (1996): *Nature* **384**, 147.

Falvo, M.R.; et al. (1997): *Nature*, 389.

Hamada, N.; Sawada, S.; Oshiyama, A. (1992): *Phys. Rev. Lett.* **68**, 1579.

Harrison, W.A. (1980): *Electronic Structure and Properties of Solids*, Freeman, San Francisco.

Louie, S.G (1996): Chemistry on the Nanometer Scale, *Proceddings of Robert A. Welch Foundation 40th Conference on Chemical Research*, Houston.

Lu, J. (1997): *Phys. Rev. Lett.* **79**, 1297.

Mintmire, J.W.; Dunlap, B.I.; White, C.T. (1992): *Phys. Rev. Lett.* **68**, 631.

Mintmire, J.W.; White, C.T. (1995): *Carbon*, **33**, 893.

Odom, T.W.; Huang, J.; Kim, P.; Lieber, C.M. (1998): *Nature*, **391**, 62.

Robertson, D.H.; Brenner, D.W.; Mintmire, J.W. (1992): *Phys. Rev. B*, **45**, 12592.

Saito, R.; Fujita, M.; Dresselhaus, G.; Dresselhaus, M.S. (1992): *Phys. Rev. B.* **46**, 1804.

Wildoer, J.W.G.; Venema, L.C.; Rinzler, A.G.; Smalley, R.E.; Dekker, C. (1998): *Nature*, **391**, 59.

Yakobsen, B.I.; Brabec, C.J.; Bernhoc, J. (1996): *Phys. Rev. Lett.* **76**, 2511.

Yang, L.; Han, J. (2000): *Phys. Rev. Lett.*, **85**, 154.

Yang, L.; Anantrum, M.P.; Han, J.; Lu, J.P. (1999): *Phys. Rev. B* **60**, 13874.